Journal of Alloys and Compounds 509 (2011) 1511–1516

Contents lists available at ScienceDirect

Journal of Alloys and Compounds

journal homepage: www.elsevier.com/locate/jallcom

Effects of Cr-addition and lamellar microstructure on the oxidation behavior of single crystal $(Mo_{0.85}Nb_{0.15})Si_2$

Ou Zhu [a], Lanting Zhang [a,*], Jinxing Yu [a], Aidang Shan [a], Jiansheng Wu [a], Koji Hagihara [b], Takayoshi Nakano [c]

[a] School of Materials Science and Engineering, Shanghai Jiao Tong University, 800 Dongchuan Rd., Shanghai 200240, China
[b] Department of Adaptive Machine Systems, Graduate School of Engineering, Osaka University, 2-1,Yamada-Oka, Suita, Osaka 565-0871, Japan
[c] Division of Materials Science and Engineering, Graduate School of Engineering, Osaka University, 2-1,Yamada-Oka, Suita, Osaka 565-0871, Japan

ARTICLE INFO

Article history:
Received 24 June 2010
Received in revised form 17 October 2010
Accepted 27 October 2010
Available online 2 November 2010

Keywords:
Transition metal alloys and compounds
Oxidation
Microstructure

ABSTRACT

The oxidation behavior of $(Mo_{0.85}Nb_{0.15})Si_2$ single crystals and the influence of Cr-addition were studied focusing on its microstructure dependence. Cr-addition to single-phase C40-structured $(Mo_{0.85}Nb_{0.15})Si_2$ crystal induced the formation of crystalline silica, leading to slightly larger weight gain during the oxidation test at 1200 °C. Furthermore, Cr-addition to C40/$C11_b$ duplex-phase $(Mo_{0.85}Nb_{0.15})Si_2$ crystal with lamellar structure strongly suppressed the internal oxidation of the $C11_b$ phase, resulting in excellent oxidation resistance. C40/$C11_b$ lamellae-structured crystals showed better oxidation resistance than the C40-structured crystals.

1. Introduction

$MoSi_2$ with $C11_b$ structure is recognized as an ideal substrate for high temperature intermetallic substrate composites. It has the excellent oxidation resistance at high temperatures [1] and is known to show plastic deformation even at low temperatures [2]. However, low temperature fracture toughness and high temperature strength above 1200 °C are still lacking in the monolithic condition [3]. Some silicides, especially $NbSi_2$ with the C40 structure are considered as the promising materials for reinforcing $MoSi_2$, because these silicides can deform plastically by the $(0\,0\,0\,1)1/3\langle 1\,\bar{2}\,1\,0]$ basal slip even at low temperatures [4]. Further, $NbSi_2$ phase is in equilibrium with $MoSi_2$ phase in a pseudo-binary phase diagram, and these two phases are fairly stable up to their melting points [5]. Recently, Nakano et al. reported that $NbSi_2/MoSi_2$ duplex silicide with a peculiar C40/$C11_b$ lamellar structure exhibited a high yield stress at ultra-high temperatures [6,7]. The aligned lamellar structure is stable during annealing at 1400 °C for 168 h [8]. Nevertheless, the thermal stability of the C40/$C11_b$ lamellar structure should be further improved for practical use. Hagihara et al. [9] further reported that the thermal stability of the lamellar microstructure could be improved by a small amount of Cr-additions. It has been demonstrated that the added Cr-atoms segregated at the C40/$C11_b$ lamellar interface.

For structural applications, oxidation resistance is another basic requirement beyond the mechanical strength. In this study, we have compared the oxidation behavior of $(Mo_{0.85}Nb_{0.15})Si_2$ and $(Mo_{0.85}Nb_{0.15})_{0.97}Cr_{0.03}Si_2$ crystals with lamellae-structured or C40-structured microstructures, in order to clarify the effect of Cr-addition and lamellar microstructure on the oxidation behavior.

2. Experimental procedure

Master ingots with nominal composition of $(Mo_{0.85}Nb_{0.15})Si_2$ and $(Mo_{0.85}Nb_{0.15})_{0.97}Cr_{0.03}Si_2$ were prepared by arc-melting high purity Mo (>99.9 wt.%), Nb (>99.9 wt.%), Cr (>99.9 wt.%), and Si (>99.9999 wt.%) under an argon atmosphere. In the latter ingot, 3 at.% of the transition atoms (Mo, Nb) were substituted with Cr atoms. The single crystals were grown in a laboratory optical-heating floating zone melting apparatus (Asgal FZ-20035WHV) at a growth rate of 2.5 mm/h. The as-grown crystals were C40 single-phase and their growth directions were approximately along $\langle 1\,0\,\bar{1}\,0\rangle$ direction. Subsequently, parts of the single crystals were encapsulated in a quartz tube and annealed at 1400 °C for 168 h to develop a fully aligned lamellar microstructure composed of C40 ($NbSi_2$) and $C11_b$ ($MoSi_2$) phases. Then, the specimens, in the form of 5 mm × 5 mm × 0.8 mm coupons, with two principal parallel plane surfaces (5 mm × 5 mm) parallel to $(1\,0\,\bar{1}\,0)$, were sectioned from the central part of the rods, for both C40-structured and lamellae-structured $(Mo_{0.85}Nb_{0.15})Si_2$ and $(Mo_{0.85}Nb_{0.15})_{0.97}Cr_{0.03}Si_2$ single crystals. Since the C40/$C11_b$ lamellar structure obeys the following crystallographic relationship, $(0\,0\,0\,1)_{C40}//(1\,1\,0)_{C11b}$, $\langle 1\,0\,\bar{1}\,0]_{C40}//[0\,0\,1]_{C11b}$ [8], the lamellar interface is actually perpendicular to the principal surfaces of the specimen. Afterwards, the specimens were metallographically polished to a 1 μm diamond finish, avoiding any inclination on the polished surface. The specimens were ultrasonically cleaned in acetone and alcohol and dried in hot air immediately before oxidation test. Isothermal oxidation was performed in air for both C40-structured and lamellae-structured $(Mo_{0.85}Nb_{0.15})Si_2$ and $(Mo_{0.85}Nb_{0.15})_{0.97}Cr_{0.03}Si_2$ single crystals at 1200 °C. The weight gain during exposure was measured by an analytical balance with a sensitivity of 10^{-6} g. After high temperature exposure, the cross-section microstructure was examined by means of scanning electron microscopy (SEM)

* Corresponding author. Tel.: +86 21 54747471; fax: +86 21 54745197.
E-mail address: lantingzh@sjtu.edu.cn (L. Zhang).

0925-8388/$ – see front matter © 2010 Elsevier B.V. All rights reserved.
doi:10.1016/j.jallcom.2010.10.138

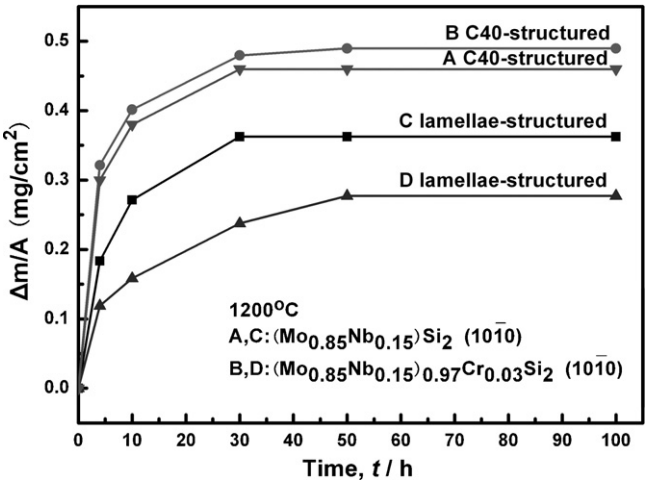

Fig. 1. Weight change as a function of exposure time in oxidation test at 1200 °C.

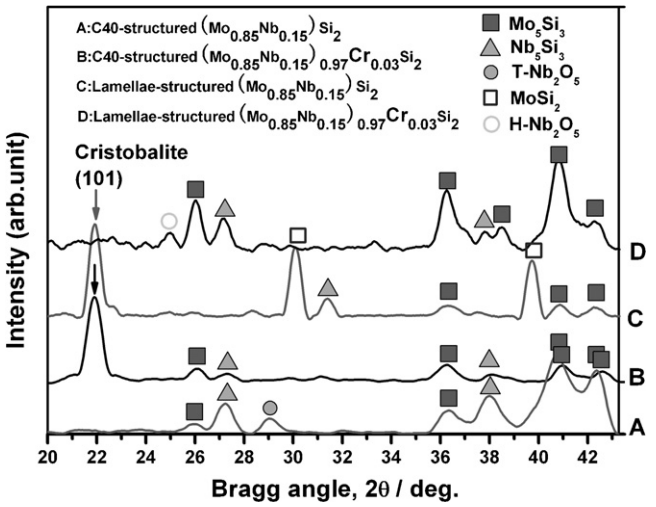

Fig. 2. X-ray diffraction patterns obtained from the surface of the specimens after oxidation at 1200 °C for 100 h.

in combination with energy-dispersive X-ray spectroscopy (EDS). The phase constitution of the oxidation products on the surface was measured by a microbeam X-ray diffractometer system (D8 Discover with GADDS, Bruker AXS) with Cu-Kα radiation (40 kV, 40 mA). The incident beam was focused onto a beam spot of 500 μm in diameter by a mono capillary collimator with a beam divergence of 0.2°. The characteristic features of the lamellar structure such as crystal orientation relationships between the constituent phases, misfit dislocations and Moiré fringes at the interfaces were examined by conventional TEM (JEOL JEM-3010, 300 kV).

3. Experimental results

3.1. Oxidation kinetics

Fig. 1 shows the weight gain of specimens during the oxidation test at 1200 °C. A near-parabolic law of oxidation weight gain was followed for both of $(Mo_{0.85}Nb_{0.15})Si_2$ and $(Mo_{0.85}Nb_{0.15})_{0.97}Cr_{0.03}Si_2$ single crystals with both of C40 structure and lamellar structure. The parabolic rate constants of all the specimens are listed in Table 1, in comparison with that of HIP-$MoSi_2$ [10]. The weight gains of all the specimens increased slowly after early stage of exposure (~10–30 h). In the C40-structured specimens, substitution of Cr for (Mo, Nb) resulted in a little higher weight gain than that of the Cr-free crystal. Meanwhile, the lamellae-structured specimens showed a much smaller weight gain than the C40-structured specimens did. Moreover, in the lamellae-structured specimens, Cr-added crystal exhibited a strong trend for reducing the weight gain, not only at the early stage but also at the stable stage of the oxidation.

3.2. Phase constitution of oxidation products

Fig. 2 shows the XRD profiles gained from the surface of the specimens after oxidation at 1200 °C for 100 h. The oxidation products were confirmed to be mainly M_5Si_3 (M = Mo, Nb) in both C40-structured and lamellae-structured $(Mo_{0.85}Nb_{0.15})Si_2$ and $(Mo_{0.85}Nb_{0.15})_{0.97}Cr_{0.03}Si_2$ single crystals on the $(1\,0\,\bar{1}\,0)_{C40}$ plane. Nevertheless, the oxides formed in the C40-structured single crystals were different depending on Cr-addition. For C40-structured crystals, the strongest peak of cristobalite phase (one type of crystalline SiO_2) was obviously detected by XRD profiles in the Cr-added crystal, but it was not found in the Cr-free crystal. This indicated that a small amount of Cr-addition in the C40-structured $(Mo_{0.85}Nb_{0.15})_{0.97}Cr_{0.03}Si_2$ single crystal assisted the formation of crystalline silica instead of the amorphous SiO_2. On the contrary, in case of the oxidation tests of the lamellae-structured specimens, the strongest peak of cristobalite could not be detected in the Cr-added crystal, while it was clearly observed in the Cr-free crystal.

Table 1
Parabolic rate constants ($mg^2\,cm^{-4}\,h^{-1}$).

	A	B	C	D	$MoSi_2$
1200 °C	2.5×10^{-3}	2.8×10^{-3}	1.8×10^{-3}	1.2×10^{-3}	1.4×10^{-4} [10]

Note: ABCD corresponds to the marks in Fig. 1.

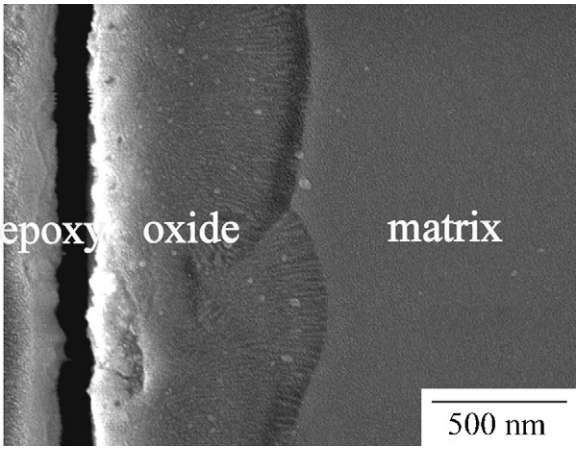

Fig. 3. Cross-section SEM image of C40-structured $(Mo_{0.85}Nb_{0.15})Si_2$ after oxidation at 1200 °C for 100 h.

3.3. Microscopic examination of oxides and substrates

The thickness of the oxide scale on all the specimens was around 0.8–0.9 μm. Fig. 3 shows the cross-section morphology of a C40-structured $(Mo_{0.85}Nb_{0.15})Si_2$ single crystal and Table 2 lists the chemical composition of the oxide scale and the matrix examined by the SEM–EDS technique. The scale was dense and exhibited good adherence to the matrix. Affinity of Si for oxygen is relatively close to that of Nb, but is much higher than that of Mo. In such silicide,

Table 2
Composition analysis of the oxide scale and the matrix (Fig. 3) in the C40-structured $(Mo_{0.85}Nb_{0.15})Si_2$ single crystal after oxidation at 1200 °C for 100 h.

(at.%)	Mo	Nb	Si	O
Oxide scale	5.1	2.4	20.2	72.3
Matrix	27.9	5.1	67.0	/

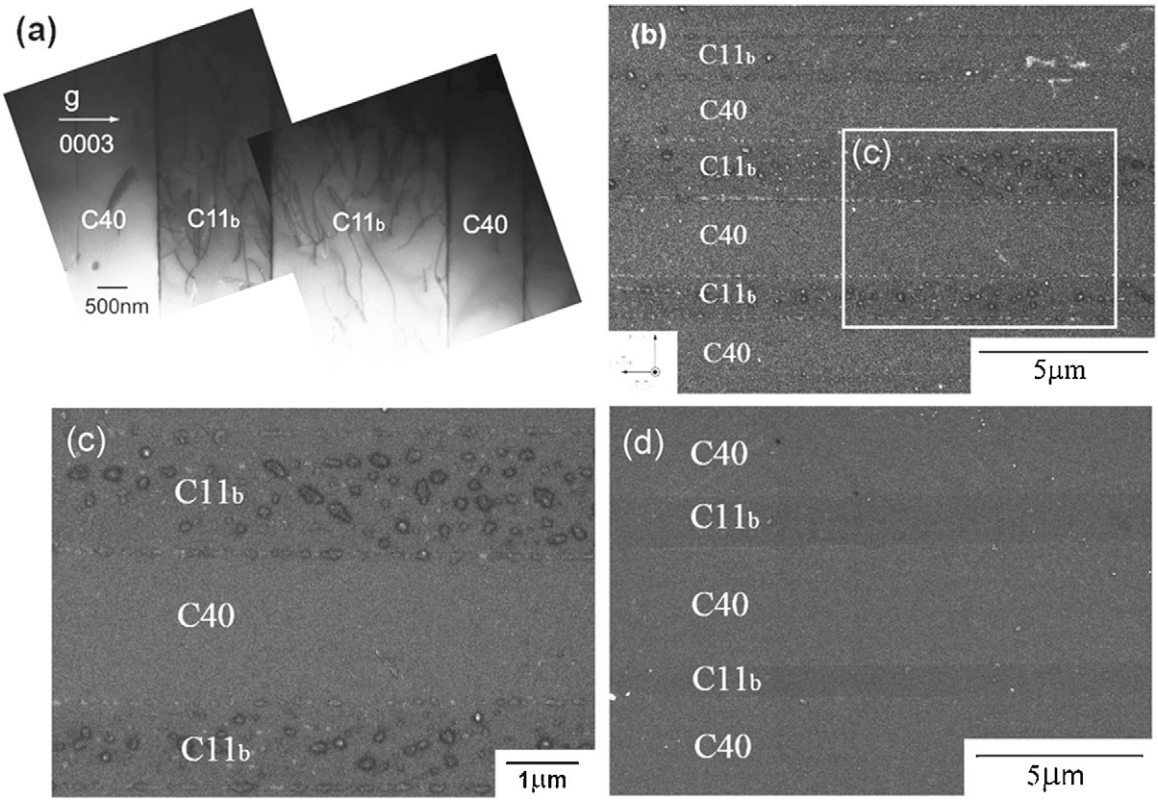

Fig. 4. (a) TEM image of the initial microstructure of the lamellae-structured $(Mo_{0.85}Nb_{0.15})Si_2$ (before oxidation), observed under the edge-on condition of the lamellar interface. (b,and c) cross-section SEM images of the lamellae-structured $(Mo_{0.85}Nb_{0.15})Si_2$ after oxidation at 1200 °C for 100 h. Part (c) is the higher magnification image of part (b). (d) Cross-section SEM image of the lamellae-structured $(Mo_{0.85}Nb_{0.15})_{0.97}Cr_{0.03}Si_2$ after oxidation at 1200 °C for 100 h.

simultaneous formation of Nb_2O_5 and SiO_2 is liable to occur, leading to a mixed oxide scale. As the atomic ratio of Si is much larger than that of Nb in the $(Mo_{0.85}Nb_{0.15})Si_2$ specimen, the oxide scale was mostly SiO_2. Although the Mo_5Si_3 and Nb_5Si_3 phases could not be clearly observed by SEM observation in this study, they were assumed to exist beneath the oxide scale, similar as it was reported in [11]. The further detailed analysis on the distribution and morphology of these phases together with Si-oxide and Nb-oxide has now been conducted by TEM–EDS method, and the results will be reported elsewhere.

Fig. 4(a) shows the microstructure of the lamellae-structured $(Mo_{0.85}Nb_{0.15})Si_2$ before oxidation test under TEM, and Fig. 4(b) and (c) shows the cross-section SEM images of the same crystal after oxidation at 1200 °C for 100 h. As clearly observed in Fig. 4(c), the dark particles of oxidation products were confirmed to be formed inside the $C11_b$ lamellae and at the lamellar interface after the oxidation test. No such particles were observed in the C40 phase before and after oxidation. Moreover, in a lower magnification image (Fig. 4(b)), some bright particles were seen aligning along the lamellar interface and a few of them were embedded inside the $C11_b$ lamellae. Nevertheless, no evidence of such dark and bright particles was found in either $C11_b$ phase or C40 phase in the Cr-added lamellae-structured crystal after oxidation at 1200 °C for 100 h, as shown in Fig. 4(d). The $C11_b$ phase and C40 phase in the lamellae-structured crystals were well distinguished by their chemical compositions (Table 3). Compared with the chemical composition of the $C11_b$ phase, the dark particles were rich in O and Si (Table 3), which indicated that the dark particles were most likely to be SiO_2. Moreover, the EDS analysis showed that the bright particles in the lamellae-structured $(Mo_{0.85}Nb_{0.15})Si_2$ were depleted in Si compared with the C40 matrix, implying that lamellar interface accelerated the diffusion of Si atoms during oxidation. In our previous paper [11], the Si-poor layer found beneath the oxide scale of $(Mo_{0.85}Nb_{0.15})Si_2$ is confirmed as a mixture of both M_5Si_3-type and M_3Si-type phases (M = Mo, Nb) after oxidation at 1400 °C for 100 h.

4. Discussion

4.1. Effect of Cr-addition on C40-structured $(Mo_{0.85}Nb_{0.15})Si_2$ crystal

Our results clearly presented the effect of $C40/C11_b$ lamellar structure and the addition of Cr on the oxidation behavior of the $(Mo_{0.85}Nb_{0.15})Si_2$ single crystals. The Cr-addition in the C40-structured $(Mo_{0.85}Nb_{0.15})_{0.97}Cr_{0.03}Si_2$ single crystal assisted the formation of crystalline silica and induced a slight increase in weight gain during oxidation. This can be understood if one considers the change in features of the initial stages of oxidation. On the oxide-free metal surface, oxides are formed of each element when the oxide formation pressure is exceeded. Oxide nuclei of SiO_2, Cr_2O_3, Nb_2O_5 and MoO_3 are expected on the surface in the initial stage on C40-structured $(Mo_{0.85}Nb_{0.15})_{0.97}Cr_{0.03}Si_2$ single crystal. After a complete oxide layer is formed, the oxygen partial pressure at the metal/oxide interface decreases to the formation pressure

Table 3
Composition analysis of the lamellae-structured $(Mo_{0.85}Nb_{0.15})Si_2$ (Cr-free) and $(Mo_{0.85}Nb_{0.15})_{0.97}Cr_{0.03}Si_2$ (Cr-added) single crystals (Fig. 4).

(at.%)	Mo	Nb	Si	O	
Cr-free crystal	$C11_b$	29.7	3.3	67.0	/
	C40	26.0	6.9	67.1	/
	Dark particle	10.2	2.6	29.9	57.3
	Bright particle	28.0	9.0	63.0	/
Cr-added crystal	$C11_b$	30.3	2.9	66.8	/
	C40	26.6	6.5	66.9	/

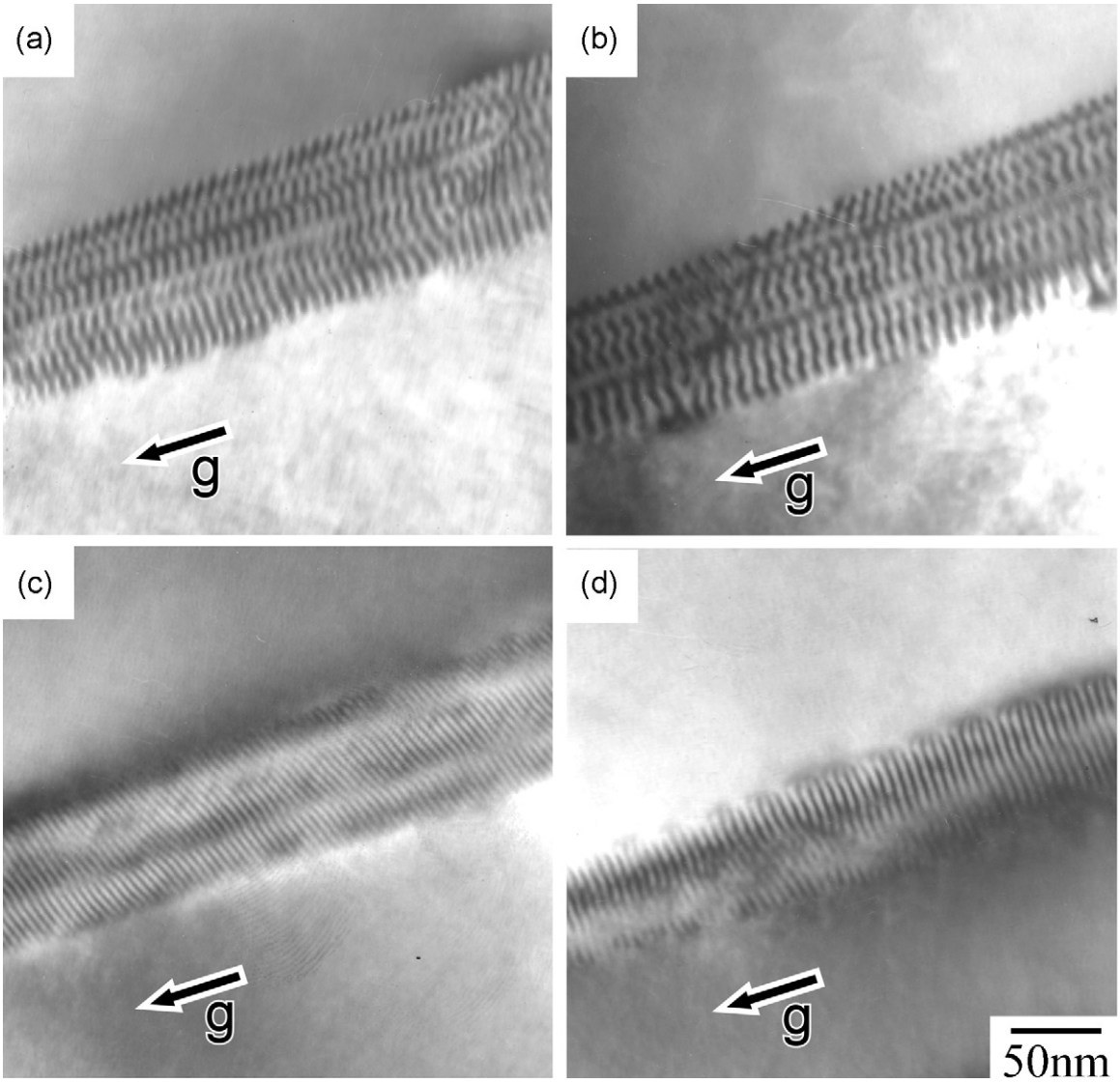

Fig. 5. Bright field images of the C40/C11$_b$ interface viewed approximately along [10-11]$_{C40}$ direction in the lamellae-structured $(Mo_{0.85}Nb_{0.15})Si_2$ crystal (a and,c) and $(Mo_{0.85}Nb_{0.15})_{0.97}Cr_{0.03}Si_2$ crystal (b and d) annealed at 1400 °C for 168 h (before oxidation). (a and b) Interfaces of C40/C11$_b$-variant1 and (c and d) interfaces of C40/C11$_b$-variant 2. The reflection vector (g) used is listed in Table 4.

of SiO_2 which is the lowest one. At this phase interface the other oxides are no longer stable and are undergrown by SiO_2. The other oxides are only stable at the gas/oxide interface. The reaction of Nb_2O_5 with Cr_2O_3 may form the tetragonal $CrNbO_4$ crystals which can act as nuclei for the formation of tetragonal cristobalite. The similar situation was found in NiAl–Cr alloy [12], in which hexagonal $(Al,Cr)_2O_3$ crystals formed in the initial stage of oxidation acts as nuclei for the formation of hexagonal α-Al_2O_3. A higher diffusion rate of O^{2-} has been reported for crystalline silica than for amorphous silica [13]. Therefore, the slightly larger weight gain in C40-structured $(Mo_{0.85}Nb_{0.15})_{0.97}Cr_{0.03}Si_2$ than in C40-structured $(Mo_{0.85}Nb_{0.15})Si_2$ (Fig. 1) can be related with the crystallization of silica. In the C40-structured specimens, the diffusion mechanism may change from O^{2-} diffusion through amorphous silica in the Cr-free crystal to lattice diffusion of O^{2-} through crystalline silica in the Cr-added crystal, and this can lead to a larger weight gain in the Cr-added crystal. It is known that lattice diffusion can dominate over grain diffusion, when temperature is above "Tamman temperature (T_a)", where $T_a \approx 2/3T_m$ (T_m – the absolute melting point)" [14]. In this study, the oxidation temperature 1200 °C is larger than the "Tamman temperature" of cristobalite at 1056 °C. Therefore, the lattice diffusion in cristobalite should be the preferential diffusion mechanism at 1200 °C.

4.2. Effect of lamellar microstructure on $(Mo_{0.85}Nb_{0.15})Si_2$ crystal

The $(Mo_{0.85}Nb_{0.15})Si_2$ crystals with lamellar microstructure can be considered as composites composing of the lamellae of C40 and C11$_b$ phases. Nakano et al. [8] showed that three variants of the C11$_b$ phase ($MoSi_2$) was produced from the C40 single crystal obeying the following crystallographic relationship, $(0\,0\,0\,1)_{C40}//(1\,1\,\bar{2}\,0)_{C11b}$, $[1\,0\,\bar{1}\,0]_{C40}//[0\,0\,1]_{C11b}$ (V1), $[1\,0\,\bar{1}\,0]_{C40}//[3\,\bar{3}\,\bar{1}]$ (V2) and $[1\,0\,\bar{1}\,0]_{C40}//[\bar{3}\,3\,\bar{1}]$ (V3). Since the crystals were cut along the $(1\,0\,\bar{1}\,0)$ plane of the C40 phase, the corresponding plane of the C11$_b$ plane is either $(0\,0\,1)$ or $(1\,\bar{1}\,\bar{2})$ or $(\bar{1}\,1\,\bar{2})$. We have measured that the weight gain on $(0\,0\,1)_{MoSi2}$ after oxidation at 1200 °C for 100 h was about 0.3 mg/cm^2, which is lower than that of C40-structured $(Mo_{0.85}Nb_{0.15})Si_2$ on $(1\,0\,\bar{1}\,0)_{C40}$ in this study. This can be responsible for the lower weight gain in C40 ($NbSi_2$)/C11$_b$ ($MoSi_2$) lamellae-structured specimens than that in C40-structured specimens. The C40/C11$_b$ lamellar interface, which is perpendicular to

Table 4
The average distance of Moiré fringes and calculated lattice misfit on the C40/C11$_b$ interface.

	Interface	Specimen	g-vector		Average distance of Moiré fringes D	Lattice misfit δ
			C40	C11$_b$		
(a)	C40-V1	$(Mo_{0.85}Nb_{0.15})Si_2$	$1\bar{2}10$	$\bar{1}10$	7.40 nm	−3.09%
(b)	$[1\bar{2}10]//[\bar{1}10]$	$(Mo_{0.85}Nb_{0.15})_{0.97}Cr_{0.03}Si_2$			8.64 nm	−2.65%
(c)	C40-V2	$(Mo_{0.85}Nb_{0.15})Si_2$	$2\bar{4}20$	$1\bar{1}6$	4.35nm	−2.63%
(d)	$[1\bar{2}10]//[11\bar{1}]$	$(Mo_{0.85}Nb_{0.15})_{0.97}Cr_{0.03}Si_2$			5.65 nm	−2.03%

the principal surface of the specimen, may provide a quick path for oxygen ions entering into the substrate, which is evidenced by the formation of silica at the lamellar interface as shown in Fig. 4(b) and (c). Moreover, it should be noted here that internal oxidation was confirmed in some C11$_b$ lamellae, and it was never found in the C40 lamellae in the lamellae-structured $(Mo_{0.85}Nb_{0.15})Si_2$. Although the origin of this internal oxidation is not fully understood yet, as one of the possibilities this may be related with the grown-in curved dislocations which were found in the C11$_b$ lamellae, but were not frequently observed in the C40 lamellae in the initial lamellae-structured crystals (Fig. 3(a)). Moreover, the large amount of grown-in dislocations in the C11$_b$ phase might also act as nucleation sites for crystallization of silica, as the dislocations can reduce the energy barrier for nucleation of silica.

Thus, the weight gain of the lamellae-structured $(Mo_{0.85}Nb_{0.15})Si_2$ single crystal is largely dependent on the weight gain of the two constituent phases. The oxidation in the C11$_b$ lamellae was largely slowed down once a complete oxide scale was formed. It is also noted that the oxidation in the C11$_b$ lamellae can be suppressed by Cr-addition in the lamellae-structured $(Mo_{0.85}Nb_{0.15})_{0.97}Cr_{0.03}Si_2$ crystal (Fig. 4(d)). Therefore, in the lamellae-structured specimens, a much smaller weight gain was obtained in the Cr-added crystal than in the Cr-free crystal (Fig. 1). This is further discussed in the following part.

4.3. Effect of Cr-addition on lamellae-structured $(Mo_{0.85}Nb_{0.15})Si_2$ crystal

Recently, it was reported by the nano-scale analytical EDS study [9] that Cr atoms in the lamellae-structured $(Mo_{0.85}Nb_{0.15})_{0.97}Cr_{0.03}Si_2$ segregated at the C40/C11$_b$ lamellar interface. We believe that the segregation of Cr atoms at the C40/C11$_b$ boundaries in the lamellae-structured $(Mo_{0.85}Nb_{0.15})_{0.97}Cr_{0.03}Si_2$ shall play a role in suppression both the silica crystallization and the rapid diffusion of oxygen ions along the lamellar interface. After oxidation, crystalline silica was induced by Cr-addition in the C40-structured $(Mo_{0.85}Nb_{0.15})Si_2$. However, in the lamellae-structured crystals, Cr atoms mainly segregated at the lamellar interface, which was perpendicular to the oxidation surface. Thus, the Cr atoms have little effect on the crystallization of silica during oxidation. In order to clarify the effect of Cr-addition on the change in lamellar interface quantitatively, the misfit strain on the interface was estimated using Moiré fringe analysis. Fig. 5 shows the bright field images of interface viewed approximately along $[10\bar{1}1]_{C40}$ direction in $(Mo_{0.85}Nb_{0.15})Si_2$ crystal (a and c) and the $(Mo_{0.85}Nb_{0.15})_{0.97}Cr_{0.03}Si_2$ crystal (b and d) with lamellar microstructures. The observation was conducted at the interfaces of C40/C11$_b$-variant1 (a and b) and C40/C11$_b$-variant 2 (c and d) [9]. Therefore, the former can clarify the misfit strain along the direction between $[10\bar{2}1]_{C40}$ and $[\bar{1}10]_{C11b}$ and the latter can explain the misfit strain between $[1\bar{2}10]_{C40}$ and $[1\bar{1}1]_{C11b}$. In the two-beam condition, two parallel reflection vectors g_{C40} in the C40 phase and g_{C11b} in the C11$_b$ phase but with slight different magnitudes were selected. The difference of the magnitude brings about the periodical oscillation of the contrast called Moiré fringes. It is known that the distance of the Moiré fringe (D) depends on the difference of the magnitude of the reflection vectors and is expressed as follows

$$D = \left(\frac{1}{|g_{C40} - g_{C11b}|} \right) = \frac{d_{C40} d_{C11b}}{d_{C40} - d_{C11b}} \quad (1)$$

where d_{C40} and d_{C11b} are the lattice parameters of the C40 and C11$_b$ phases, respectively. With the value D, the misfit strain δ at the vicinity of interface can be estimated by the following equation

$$\delta = 2\left(\frac{d_{C11b} - d_{C40}}{d_{C11b} + d_{C40}} \right) \times 100 = \frac{-2d_{C40}^2}{2Dd_{C40} + d_{C40}^2} \times 100 \quad (2)$$

As shown in Fig. 5, period of contrast oscillations within the Moiré fringe pattern is much wider in the $(Mo_{0.85}Nb_{0.15})_{0.97}Cr_{0.03}Si_2$ crystal than that in the $(Mo_{0.85}Nb_{0.15})Si_2$ crystal, indicating that the lattice mismatch is effectively decreased by Cr-additions. Table 4 lists the results of the quantitative analysis on the average distance of the Moiré fringe and calculated misfit strain. The results clearly demonstrate that the segregation of the Cr-atoms induced about 14–23% reduction of misfit strain at the lamellar interface. Therefore, the segregated Cr-atoms at the lamellar interface were stable during the whole oxidation period at 1200 °C. These segregated Cr atoms at the lamellar interface are expected to act as a strong obstacle against the oxygen ions diffusion along the lamellar interface into the substrate. This reduces the internal oxidation of the C11$_b$ lamellae, resulting in the lowest weight gain of lamellae-structured $(Mo_{0.85}Nb_{0.15})_{0.97}Cr_{0.03}Si_2$ crystal during the oxidation test.

5. Conclusions

In this study, we have explored the oxidation behavior of the C40-structured and lamellae-structured $(Mo_{0.85}Nb_{0.15})Si_2$ and $(Mo_{0.85}Nb_{0.15})_{0.97}Cr_{0.03}Si_2$ single crystals at 1200 °C. Obtained results were summarized as follows:

1. Lamellae-structured specimens exhibited better oxidation resistance than the C40-structured specimens. This can be related to the better oxidation resistance of the C11$_b$ phase than that of the C40 phase. Lamellae-structured $(Mo_{0.85}Nb_{0.15})_{0.97}Cr_{0.03}Si_2$ single crystal on $(10\bar{1}0)_{C40}$ crystallographic plane displayed excellent oxidation resistance.

   A small amount of Cr-additions to C40-structured $(Mo_{0.85}Nb_{0.15})Si_2$ single crystal assisted crystallization of silica, which in turn led to a slightly larger weight gain than the Cr-free C40-structured crystal during the oxidation test.
2. Internal oxidation in the C11$_b$ lamellae was found in the lamellae-structured $(Mo_{0.85}Nb_{0.15})Si_2$ single crystal, but not in the lamellae-structured $(Mo_{0.85}Nb_{0.15})_{0.97}Cr_{0.03}Si_2$ single crystal.
3. Cr segregation at the lamellar interface in the lamellae-structured $(Mo_{0.85}Nb_{0.15})_{0.97}Cr_{0.03}Si_2$, may suppress both crystallization of silica and the diffusion of oxygen ions along the lamellar interface. The internal oxidation of the C11$_b$ lamellae is thus reduced, resulting in the lowest weight gain among all the tested specimens

Acknowledgements

This study is supported by the National Natural Science Foundation of China (#50571067), the Science and Technology Committee of Shanghai Municipal Government (#05PJ14072), "Priority Assistance of the Formation of Worldwide Renowned Centers of Research — The Global COE Program (Project: Center of Excellence for Advanced Structural and Functional Materials Design)," and a Grant-in-Aid for Scientific Research and Development from the Ministry of Education, Culture, Sports, Science and Technology of Japan. SEM observations in this study were carried out at the Instrumental Analysis Center at Shanghai Jiao Tong University.

References

[1] R. Mitra, Int. Mater. Rev. 51 (2006) 13.
[2] K. Ito, H. Inui, Y. Shirai, M. Yamaguchi, Phil. Mag. A 72 (1995) 1075.
[3] J.J. Petrovic, A.K. Vasudevan, Mater. Sci. Eng. A 261 (1999) 1.
[4] Y. Umakoshi, T. Nakano, E. Yangisawa, T. Takezoe, A. Negishi, Mater. Sci. Eng. 102 (1997) A239–A240.
[5] W.J. Boettinger, J.H. Perepezko, P.S. Frankwicz, Mater. Sci. Eng. A155 (1992) 33.
[6] T. Nakano, M. Azuma, Y. Umakoshi, Intermetallics 6 (1998) 715.
[7] T. Nakano, K. Hagihara, Y. Nakai, Y. Umakoshi, Intermetallics 14 (2006) 1345.
[8] T. Nakano, Y. Nakai, S. Maeda, Y. Umakoshi, Acta Mater. 50 (2002) 1781.
[9] K. Hagihara, T. Nakano, S. Hata, O. Zhu, Y. Umakoshi, Scripta Mater. 62 (2010) 613.
[10] S. Melsheimer, M. Fietzek, V. Kolarik, A. Rahmel, M. Schütze, Oxid. Met. 47 (1997) 139.
[11] L.T. Zhang, O. Zhu, F. Zhang, A.D. Shan, J.S. Wu, Scripta Mater. 57 (2007) 305.
[12] M.W. Brumm, H.J. Grabke, Corros. Sci. 33 (1992) 1677.
[13] K. Kurokawa, D. Goto, J. Kuchino, A. Yamauchi, T. Shibayama, H. Takahashi, Mater. Sci. Forum 522 (2006) 595.
[14] P.G. Shewmon, Diffusion in Solid, McGraw-Hill [M], New York, 1963.